16th World Conference on Earthquake, 16WCEE 2017

Santiago Chile, January 9th to 13th 2017

Paper N° 3427

Registration Code: S-Q1464752830

SIMULATION OF AN RC BRIDGE COLUMN SHAKE-TABLE TEST USING A FIBER BEAM-COLUMN MODEL CONSIDERING REINFORCEMENT ANCHORAGE SLIP

W. H. Pan[(1)], M. X. Tao[(2)], J. G. Nie[(3)]

[(1)] *Ph. D. Candidate, Department of Civil Engineering, Tsinghua University, 10084 Beijing, China, panwenhao13@tsinghua.org.cn*
[(2)] *Assistant Professor, Department of Civil Engineering, Tsinghua University, 10084 Beijing, China, taomuxuan@tsinghua.edu.cn*
[(3)] *Professor, Department of Civil Engineering, Tsinghua University, 10084 Beijing, China, niejg@tsinghua.edu.cn*

Abstract

Reinforcement slip in footing can make a significant contribution to the total lateral displacement of a reinforced concrete (RC) column, and thereby greatly influenced the seismic responses. In this paper, to simulate a flexure-dominated RC bridge column shake-table test, a modified fiber beam-column element model considering reinforcement slip in footing is developed and implemented in a general commercial finite element (FE) package. First, on the basis of an effective macro model for calculating anchorage slip and a classical uniaxial stress–strain relationship of rebar, the reinforcement anchorage slip in the footing is formulated. The macro model assumed a stepped bond stress to deal with the bond–slip relationship, and the slip is derived by integrating the strain over the development length. Then, the derived anchorage slip is introduced into the framework of the conventional fiber element model. By considering the rebar fiber strain in the footing fiber element as the sum of the rebar deformation and the anchorage slip, the stress–strain skeleton curve and the hysteretic law of rebar are modified. Finally, the shake-table test of a full-scale flexure-dominated bridge column is simulated to validate the developed model. Comparisons indicate the considerably improved accuracy of the developed model in simulating the column displacement time-histories, base moment–column displacement responses, and base moment–base curvature responses. The developed model shows good accuracy in simulating the moment capacity and column stiffness, whereas the conventional fiber model significantly overestimates the column lateral stiffness. In addition, the measured lateral displacement ratio caused by the fixed-end rotation in each test is well predicted by the developed model. Therefore, the model is validated at structural, sectional and micro levels.

Keywords: Shake-table test; Fiber beam–column element model; Reinforcement anchorage slip; Fixed-end rotation

1. Introduction

A 1.22-m diameter, 7.32-m height full-scale RC bridge column (Fig. 1) was tested under simulated ground motions produced by the NEES shake table at the University of California, San Diego [1–4]. To response in the nonlinear range with a flexure-dominated behavior, the column was designed to have a moment-to-shear ratio of 6*D* (*D* is the column diameter). A total of ten earthquake simulation tests were conducted. The results in the first six tests were provided for a blind prediction competition [2, 3]. These test results could serve as a unique dataset that can be used to validate nonlinear finite element models.

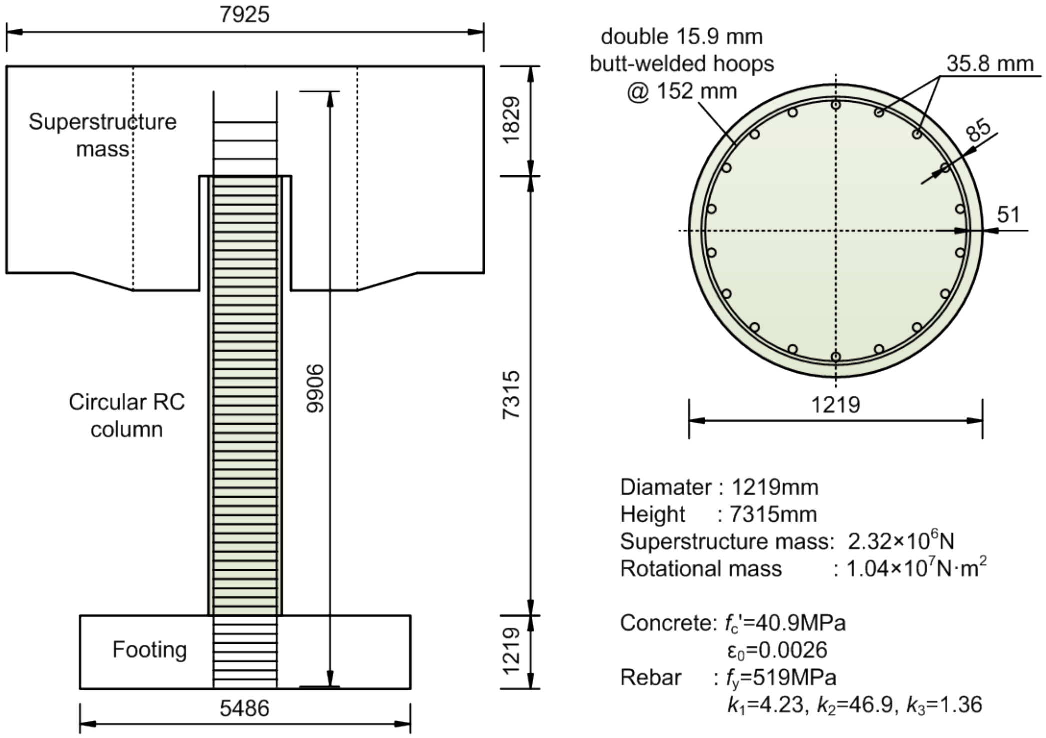

Fig. 1 – Column geometry and material properties

Reinforcement anchorage slip in the footing can make a significant contribution to the total lateral displacement of a reinforced concrete (RC) column [5–7]. A reinforcing rebar embedded in the footing will accumulate strain over the development length under tensile load. The accumulation of this strain will cause the rebar to extend, thereby causing anchorage slip at the column–footing interface. The anchorage slip in the tensile region of a column section will cause fixed-end rotation of the column, which may notably increase the lateral displacement of the column. Experimental results from the bridge column shake-table test indicated that the fixed-end rotation contributed approximately 15% of the total lateral displacement [1] and thereby significantly influence the seismic responses. For columns with longitudinal reinforcement in worse anchorage conditions, the contribution of slip deformations may be as large as flexural deformations [5]. Therefore, for better prediction of the column responses in the shake-table test, anchorage slip is needed to be considered in the numerical model.

Researchers have made significant efforts to model this anchorage slip effect [6–14]. However, few of these models can be directly integrated in the framework of the fiber beam–column element model [15–18], which is popularized in professional engineering practice because of its high accuracy and low computational effort. Because of the lack of efficient fiber beam-column element model for simulating the complex anchorage slip effect, a simple and computationally efficient fiber model considering the anchorage slip effect is developed and implemented in a general commercial FE package, MSC.MARC (2012) [19]. The developed model is then applied to simulate the full-scale RC bridge column shake-table test by PEER. The experimental results of the column displacement time-histories, base moment–column displacement responses, and base moment–base curvature responses are compared with the numerical results, which are obtained with and without considering anchorage slip effect. In addition, the numerical results of the lateral displacement ratio caused by fixed-end rotation are compared with the experimental results to further validate the developed model.

2. Fiber beam–column element model considering anchorage slip

2.1 Conventional fiber model

Assuming that plane sections remain plane and normal to the longitudinal axis, the sectional constitutive law can be derived from the material uniaxial models under the framework of the fiber element model. Therefore, the uniaxial constitutive laws of fiber materials play a significant role in the rational prediction of structural nonlinear responses. As the basis of this study, a conventional fiber model developed in previous studies [17, 18] is first introduced.

The uniaxial stress–strain skeleton curve and hysteretic law of concrete are shown in Fig. 2. For the concrete in compression, the stress–strain (σ–ε) relationship assumes a parabolic form before the peak compressive strain ε_0. When the compressive strain ε exceeds the peak compressive strain ε_0, a linear relationship is assumed for ordinary concrete. For concrete in tension, a bilinear model is assumed. Concrete demonstrates evident strength and stiffness degradation effects under cyclic loading. Therefore, for the uniaxial stress–strain hysteretic law of concrete, an elaborated model that can effectively consider these two significant effects is applied [18].

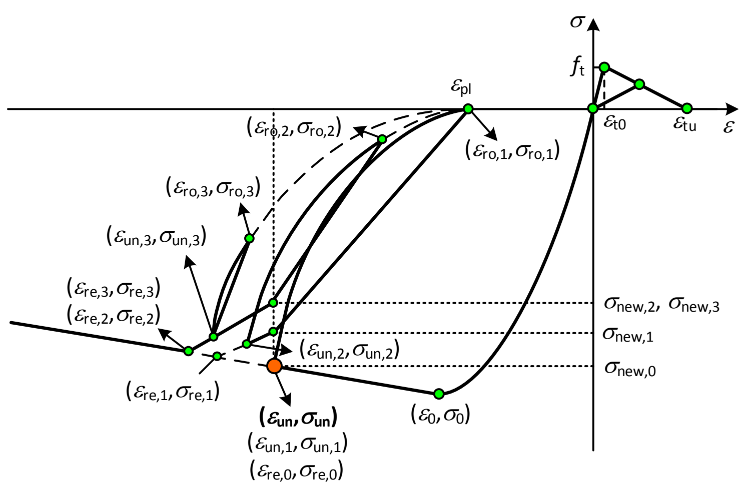

Fig. 2 – Uniaxial constitutive laws of concrete

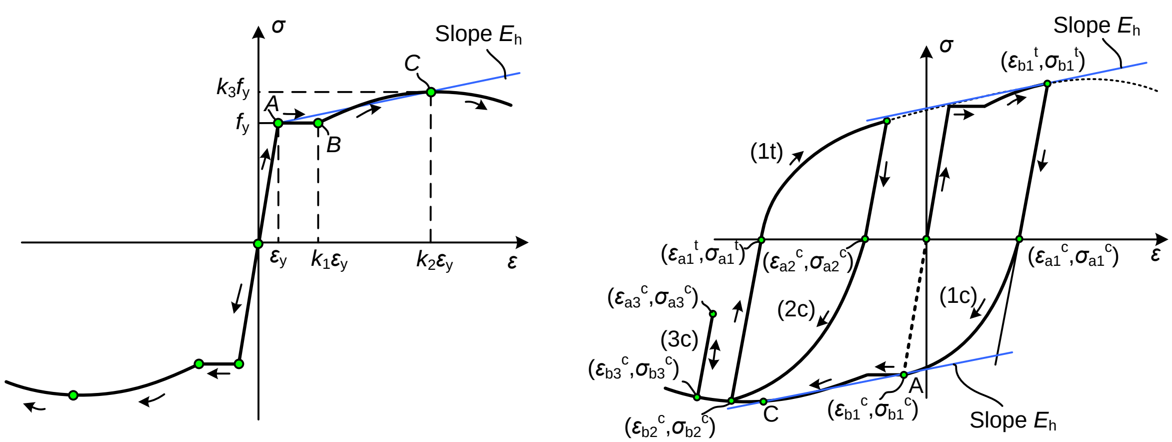

(a) Skeleton curve (b) Hysteretic law

Fig. 3 – Uniaxial constitutive laws of rebar (σ–ε_s relation)

The referenced uniaxial stress–strain skeleton curve of rebar [20] is formulated in Eq. (1) and shown in Fig. 3a. In the elastic and yielding ranges, the stress–strain relationships are typical for sharp yielding steels. The elastic modulus E_s is set to 200,000 MPa. In the strain hardening range, the stress–strain relationship is assumed to have a parabolic form. In addition, three factors k_1, k_2, and k_3 are applied to define the shape of the uniaxial stress–strain skeleton curve. In this study, attentions are focused on the anchorage slip and its influence on the rebar constitutive laws; thus, other effects such as the complex buckling and degradation of rebar in compression is not considered.

$$\sigma = \begin{cases} E_s\varepsilon & (0 < \varepsilon \le \varepsilon_y) \\ f_y & (\varepsilon_y < \varepsilon \le k_1\varepsilon_y) \\ k_3 f_y + \dfrac{E_s(1-k_3)}{\varepsilon_y(k_2-k_1)^2}(\varepsilon - k_2\varepsilon_y)^2 & (k_1\varepsilon_y < \varepsilon) \end{cases} \tag{1}$$

where f_y denotes the yielding stress; and ε_y denotes the yielding strain.

The hysteretic law of rebar is shown in Fig. 3b. The classical elastic unloading rule is assumed, and the unloading modulus is equal to the elastic modulus E_s. For the reloading rule, an elaborated law that has a good accuracy in simulating the nonlinear kinematic hardening is adopted [21], as formulated in Eq. (2). As shown in Fig. 3b, a beginning point and an end point are defined to determine the i-th reloading curve. If the slope from the beginning point to the end point is less than E_s, a p-power curve is assumed (refer to the reloading branches (1c), (1t), and (2c) in Fig. 3b. Power p should be determined according to Eq. (3); thus, the slopes of the reloading curve at the beginning point and the end point are equal to E_s and E_h, respectively.

$$E_s\left(\varepsilon - \varepsilon_{ai}^{t/c}\right) - \left(\sigma - \sigma_{ai}^{t/c}\right) = \begin{cases} \left[E_s\left(\varepsilon_{bi}^{t/c} - \varepsilon_{ai}^{t/c}\right) - \left(\sigma_{bi}^{t/c} - \sigma_{ai}^{t/c}\right)\right]\cdot\left(\dfrac{\varepsilon - \varepsilon_{ai}^{t/c}}{\varepsilon_{bi}^{t/c} - \varepsilon_{ai}^{t/c}}\right)^p & \left(E_s\left(\varepsilon_{bi}^{t/c} - \varepsilon_{ai}^{t/c}\right) > \sigma_{bi}^{t/c} - \sigma_{ai}^{t/c}\right) \\ 0 & \left(E_s\left(\varepsilon_{bi}^{t/c} - \varepsilon_{ai}^{t/c}\right) \le \sigma_{bi}^{t/c} - \sigma_{ai}^{t/c}\right) \end{cases} \tag{2}$$

$$p = \frac{E_s\left(1 - E_h/E_s\right)\left(\varepsilon_{bi}^{t/c} - \varepsilon_{ai}^{t/c}\right)}{E_s\left(\varepsilon_{bi}^{t/c} - \varepsilon_{ai}^{t/c}\right) - \left(\sigma_{bi}^{t/c} - \sigma_{ai}^{t/c}\right)} \tag{3}$$

where E_h denotes the hardening modulus defined in Fig. 3a.

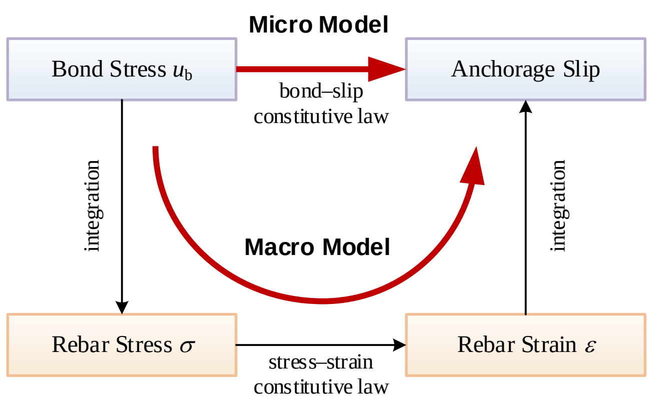

Fig. 4 – Micro and macro models for calculating anchorage slip

2.2 Anchorage slip in the footing

Numerous numerical models for calculating anchorage slip have been put forward by researchers. As shown in Fig. 4, Micro models [9-11] consider the bond stress–anchorage slip relationship directly, whereas macro models [6, 7] deal with the bond–slip relationship in an average way and a stepped bond stress is often assumed. Although micro models seem to be straightforward, they may require a high computational effort in an iteration process. On the contrary, with simple assumptions, macro models are often very effective from a computational viewpoint. Among all available models for calculating anchorage slip in the footing, this study applies the macro model proposed by Sezen and Setlzer [7], which predicts slip displacements reasonably well considering its simplicity and computational efficiency.

Fig. 5 shows a reinforcing rebar embedded in the footing under tensile load. The rebar is assumed to have a sufficient anchorage length, which is able to provide a full anchorage strength. As shown in Fig. 5, the bond stress is approximated as a stepped function, and is given by u_b for elastic rebar stress and $u_b' = 0.5u_b$ for inelastic rebar stress. On the basis of this assumption, the rebar stress distribution can be derived by integrating the bond stress over the development length. Then, the rebar strain distribution can be derived according to the uniaxial stress–strain relationship of rebar (Fig. 3a). Finally, the slip can be derived (Eq. (4)) by integrating the strain over the development length l_d, as shown in the shaded area of Fig. 5.

$$\mathrm{slip} = \int_0^{l_d} \varepsilon(x)dx \tag{4}$$

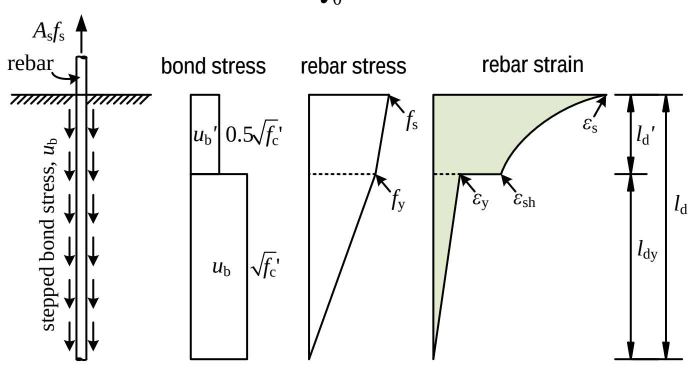

Fig. 5 – Anchorage slip model proposed by Sezen and Setlzer [7]

The development length l_d is derived from the equilibrium of forces along the rebar, as shown in Eq. (5).

$$l_d = \begin{cases} \dfrac{f_s d_b}{4u_b} & (f_s \le f_y) \\ l_{dy} + l_d' = \dfrac{f_y d_b}{4u_b} + \dfrac{(f_s - f_y)d_b}{4u_b'} & (f_s > f_y) \end{cases} \tag{5}$$

where f_s denotes the rebar stress; and d_b denotes the rebar diameter.

Carrying out the integration of Eq. (4), the anchorage slip is derived as Eq. (6). In addition, the anchorage slip under two typical stress levels, i.e. the yielding stress f_y and the ultimate stress f_u, is formulated as Eqs. (7) and (8).

$$\mathrm{slip} = \begin{cases} \dfrac{\varepsilon_s l_d}{2} & (\varepsilon_s \le \varepsilon_y) \\ \mathrm{slip}_y + \mathrm{slip}' = \dfrac{\varepsilon_y l_{dy}}{2} + \displaystyle\int_{l_{dy}}^{l_{dy}+l_d'} \varepsilon(x)dx & (\varepsilon_s > \varepsilon_y) \end{cases} \tag{6}$$

$$\text{slip}_{\text{y}} = \frac{\varepsilon_{\text{y}} l_{\text{dy}}}{2} \tag{7}$$

$$\text{slip}_{u} = \text{slip}_{\text{y}} + \text{slip}_{\text{sh}} = \frac{\varepsilon_{\text{y}} l_{\text{dy}}}{2} + \varepsilon_{\text{y}} \cdot \frac{f_{\text{y}} d_{\text{b}}}{4u_{\text{b}}'}(k_3 - 1) \cdot \left(\frac{2}{3}k_1 + \frac{1}{3}k_2\right) \tag{8}$$

2.3 Modified fiber model

According to Monti and Spacone [10], to consider anchorage slip in the footing, the fiber element model retains the plane-section assumption, but the rebar fiber strain in the footing fiber element is computed as the sum of two contributions: the rebar deformation and the anchorage slip. The anchorage slip is assumed to be uniformly distributed in the rebar fiber of the footing element. On the basis of these assumptions, the slip-induced rebar fiber strain $\varepsilon_{\text{slip}}$ and the total rebar fiber strain $\varepsilon_{\text{total}}$ in the footing fiber element can be determined as Eqs. (9) and (10). Then, the stress–total strain (σ–$\varepsilon_{\text{total}}$) relationship is assumed for the modified uniaxial constitutive law of rebar in the footing fiber element. Therefore, the fiber model considering reinforcement slip can be developed.

$$\varepsilon_{\text{slip}} = \frac{\text{slip}}{L_{\text{e}}} \tag{9}$$

$$\varepsilon_{\text{total}} = \varepsilon_{\text{s}} + \varepsilon_{\text{slip}} \tag{10}$$

where L_{e} denotes the length of the footing fiber element; and slip denotes the rebar anchorage slip.

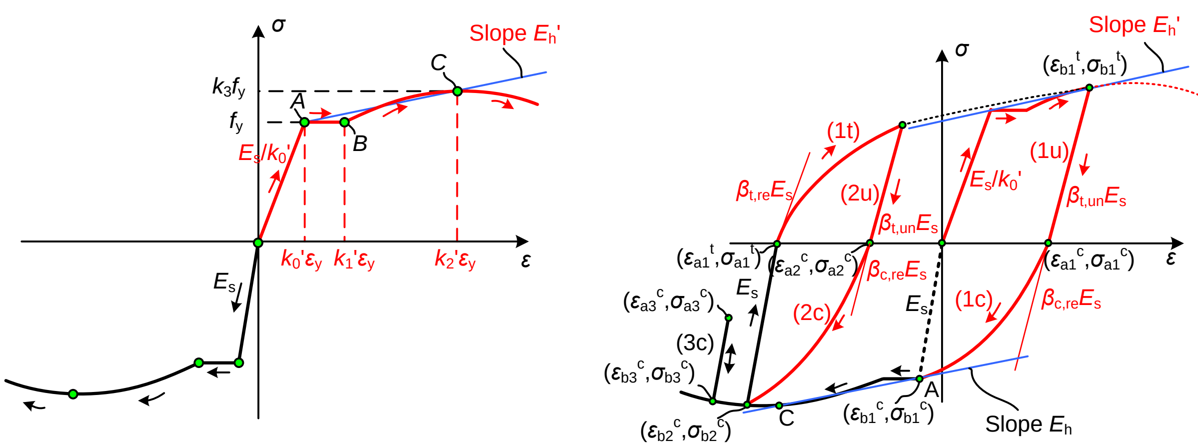

(a) Skeleton curve (b) Hysteretic law

Fig. 6 – Modified constitutive laws of rebar (σ–$\varepsilon_{\text{total}}$ relation)

Following this σ–$\varepsilon_{\text{total}}$ process and the formulated anchorage slip in the footing, the uniaxial stress–strain skeleton curve of rebar is modified for the footing fiber element, as shown in Fig. 6a and formulated in Eq. (11). All modifications relative to Fig. 3 are marked in red. Because anchorage slip develops as rebar stress increases in the elastic and hardening ranges, the modification in the skeleton curve is the elastic stiffness of rebar and the elongation of the hardening branch under tensile loading. For simplicity and effectiveness, the modified formula for the stress–strain skeleton curve follows the original form, and the rebar strain of the three typical points A, B, and C are increased as formulated in Eqs. (12–14). Because zero anchorage slip is assumed for rebar under compressive loading, the compressive part of the skeleton curve remains unchanged.

$$\sigma = \begin{cases} E_s\varepsilon / k_0' & (0 < \varepsilon \le k_0'\varepsilon_y) \\ f_y & (k_0'\varepsilon_y < \varepsilon \le k_1'\varepsilon_y) \\ k_3 f_y + \dfrac{E_s(1-k_3)}{\varepsilon_y(k_2'-k_1')^2}(\varepsilon - k_2'\varepsilon_y)^2 & (k_1'\varepsilon_y < \varepsilon \le k_2'\varepsilon_y) \\ k_3 f_y + \dfrac{E_s(1-k_3)}{\varepsilon_y(k_2-k_1)^2}(\varepsilon - k_2'\varepsilon_y)^2 & (k_2'\varepsilon_y < \varepsilon) \end{cases} \tag{11}$$

where k_0', k_1', and k_2' denote the three factors defining the shape of the modified uniaxial stress–strain skeleton curve, and they can be formulated as Eqs. (12–14) according to Eqs. (9) and (10).

$$k_0' = 1 + \alpha_y \tag{12}$$

$$k_1' = k_1 + \alpha_y \tag{13}$$

$$k_2' = k_2 + \alpha_y + \alpha_{sh} \tag{14}$$

where α_y and α_{sh} denote the strain incremental factors for the elastic range and the hardening range of the rebar, respectively.

$$\alpha_y = \frac{f_y d_b}{8 u_b L_e} \tag{15}$$

$$\alpha_{sh} = \frac{f_y d_b}{4 u_b' L_e}(k_3 - 1)\cdot\left(\frac{2}{3}k_1 + \frac{1}{3}k_2\right) \tag{16}$$

The modified hysteretic law is shown in Fig. 6b. The reloading rule is further formulated in Eqs. (17) and (18). To consider anchorage slip effect, the unloading modulus and the initial reloading modulus are reduced according to Eqs. (9) and (10). The reduction factors with respect to tensile/compressive unloading and reloading are formulated in Eq. (19).

$$\beta_{c/t,re} E_s\left(\varepsilon - \varepsilon_{ai}^{t/c}\right) - \left(\sigma - \sigma_{ai}^{t/c}\right) = \begin{cases} \left[\beta_{c/t,re} E_s\left(\varepsilon_{bi}^{t/c} - \varepsilon_{ai}^{t/c}\right) - \left(\sigma_{bi}^{t/c} - \sigma_{ai}^{t/c}\right)\right]\cdot\left(\dfrac{\varepsilon - \varepsilon_{ai}^{t/c}}{\varepsilon_{bi}^{t/c} - \varepsilon_{ai}^{t/c}}\right)^p & \left(\beta_{c/t,re} E_s\left(\varepsilon_{bi}^{t/c} - \varepsilon_{ai}^{t/c}\right) > \sigma_{bi}^{t/c} - \sigma_{ai}^{t/c}\right) \\ 0 & \left(\beta_{c/t,re} E_s\left(\varepsilon_{bi}^{t/c} - \varepsilon_{ai}^{t/c}\right) \le \sigma_{bi}^{t/c} - \sigma_{ai}^{t/c}\right) \end{cases} \tag{17}$$

$$p = \frac{\beta_{c/t,re} E_s\left(1 - E_h' / \beta_{c/t,re} E_s\right)\left(\varepsilon_{bi}^{t/c} - \varepsilon_{ai}^{t/c}\right)}{\beta_{c/t,re} E_s\left(\varepsilon_{bi}^{t/c} - \varepsilon_{ai}^{t/c}\right) - \left(\sigma_{bi}^{t/c} - \sigma_{ai}^{t/c}\right)} \tag{18}$$

$$\beta=\begin{cases}\beta_{\mathrm{t,un}}=\left(1+\dfrac{0.5\alpha_{\mathrm{y}}\varepsilon_y+R_1\left(\varepsilon_{\mathrm{slip,max}}-\alpha_{\mathrm{y}}\varepsilon_y\right)}{\varepsilon_y}\right)^{-1} & \text{(tensile unloading)}\\ \beta_{\mathrm{t,re}}=\left(1+\dfrac{1.0\alpha_{\mathrm{y}}\varepsilon_y+R_2\left(\varepsilon_{\mathrm{slip,max}}-\alpha_{\mathrm{y}}\varepsilon_y\right)}{\varepsilon_y}\right)^{-1} & \text{(tensile reloading)}\\ \beta_{\mathrm{c,un}}=1 & \text{(compressive unloading)}\\ \beta_{\mathrm{c,re}}=\beta_{\mathrm{t,un}} & \text{(compressive reloading)}\end{cases} \tag{19}$$

where $\varepsilon_{\mathrm{slip,max}}$ denotes the maximum experienced slip strain and is set to the yielding slip strain $\alpha_y\varepsilon_y$ when rebar has not reached the tensile yielding stress; and R_1 and R_2 denote the degree of anchorage slip recovery/development in the strain hardening range of rebar during tensile unloading and tensile reloading, respectively.

2.4 Post-processing for fixed-end rotation ratio

After the finite element analysis, a post-processing method can be applied to derive the lateral displacement ratio caused by the fixed-end rotation owing to the anchorage slip effect (denoted by the fixed-end rotation (FER) ratio R_{FER}). Following a reverse process of the total rebar strain ($\varepsilon_{\mathrm{total}}$) determination shown in Eqs. (9) and (10), the fixed-end rotation ratio is formulated in Eq. (22) after solving the anchorage slip and the slip rotation angle θ_{FER}.

$$\text{slip}=L_{\mathrm{e}}\varepsilon_{\mathrm{slip}}=L_{\mathrm{e}}\left(\varepsilon_{\mathrm{total}}-\varepsilon_{\mathrm{s}}\right) \tag{20}$$

$$\theta_{\mathrm{FER}}=\frac{\text{slip}_{\mathrm{t}}-\text{slip}_{\mathrm{c}}}{d_{\mathrm{t}}-d_{\mathrm{c}}} \tag{21}$$

$$R_{\mathrm{FER}}=\frac{L\theta_{\mathrm{FER}}}{\Delta} \tag{22}$$

where slip_{t} and slip_{c} denote the anchorage slip in the extreme tension and compression rebar, respectively; $d_{\mathrm{t}}-d_{\mathrm{c}}$ denotes the distance between the extreme tensile and compressive rebars; and Δ denotes the top lateral displacement.

3. Simulation of the RC bridge column shake-table test

3.1 Experiment and modeling

The test specimen included a circular RC column, superstructure mass, and a footing, as shown in Fig. 1. The column had a longitudinal reinforcement ratio of 1.55% and a transverse reinforcement volumetric confining ratio of 0.95%. The superstructure mass weighing 2.32×10^6 N was cast on top of the bridge column to mobilize inertia forces, which also produced an axial load ratio of $5.3\%A_{\mathrm{g}}f_{\mathrm{c}}'$ at the column base. A sufficient anchorage length of one column diameter was designed for the longitudinal reinforcements to the footing, which was rigidly post-tensioned to the shake table. Fig. 1 also shows the material properties.

In the finite element modeling, the element mesh and section discretization are shown in Fig. 7. As shown in Fig. 7a, the developed fiber model considering the anchorage slip is applied to the footing fiber element only, while the conventional fiber model is applied to the upper fiber elements. To accurately consider the deformation localization effect [22] in displacement-based fiber models, the rational mesh size is selected as the equivalent plastic hinge length L_{p} of a cantilevered member. For the equivalent plastic hinge length L_{p} of an RC column with a low axial load ratio, the formula recommended by Zahn [23] (Eq. (23)) is applied. In addition, to ensure accuracy in professional engineering practice [18], 80 concrete section fibers resulting from 16 circumferential divisions and 5 radial divisions are applied.

$$L_{\mathrm{p}} = (0.08L + 6d_{\mathrm{b}})\left(0.5 + 1.67\frac{P}{f'_{\mathrm{c}}A_{\mathrm{g}}}\right) \quad \left(\frac{P}{f'_{\mathrm{c}}A_{\mathrm{g}}} < 0.3\right) \tag{23}$$

where L denotes the column height; P denotes the axial load; and A_{g} denotes the gross cross-sectional area of the column.

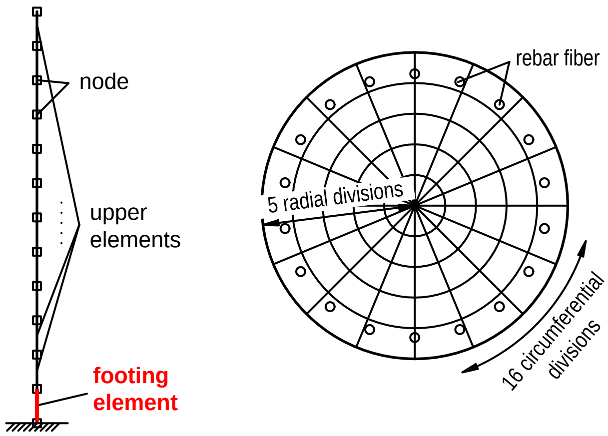

(a) Element mesh (b) Section discretization

Fig. 7 – Element mesh and section discretization

3.2 Column responses

Fig. 8 compares the measured column displacement time-histories with the numerical results. To exclude the accumulated error in earlier earthquake simulation tests, the column displacement numerical results are shifted such that the initial column displacement numerical result is the same as the experimental result for each test. Comparisons between the numerical and test results indicate the good accuracy of the developed model considering anchorage slip effect in simulating the column displacement time-history response at the early stage of each earthquake simulation test. On the contrary, the conventional model without considering the slip effect may significantly underestimate or overestimate the column responses during low-intensity earthquakes, as shown in EQ1 (Fig. 8a). Additionally, as shown in Fig. 8, the developed model can also predicts the peak column displacements better. In general, the developed model is able to predict the column responses with a considerably improved accuracy. Therefore, anchorage slip effect should be considered while simulating RC column responses under earthquakes.

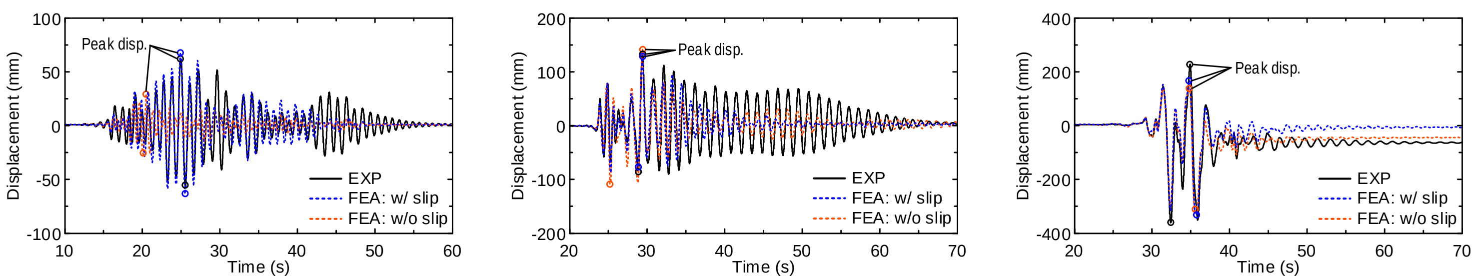

(a) EQ1 (b) EQ2 (c) EQ3

Fig. 8 – Comparison of column displacement time-histories

Fig. 9 compares the measured column responses in terms of base moment and top lateral displacement with the numerical results. Comparisons indicate the good accuracy of the developed model in simulating the column responses at a structural level. The developed model can closely predict the column stiffness, indicating that the lateral displacement contributed by the anchorage slip are well considered. Therefore, the modified fiber element model is validated at the structural level. On the contrary, the conventional model without considering the slip effect overestimates the column lateral stiffness, and thus may underestimate or overestimate the column responses during some earthquakes, especially in EQ1 and EQ2 (Figs. 9a and b). Therefore, anchorage slip effect should be considered while simulating RC column structural responses under earthquakes.

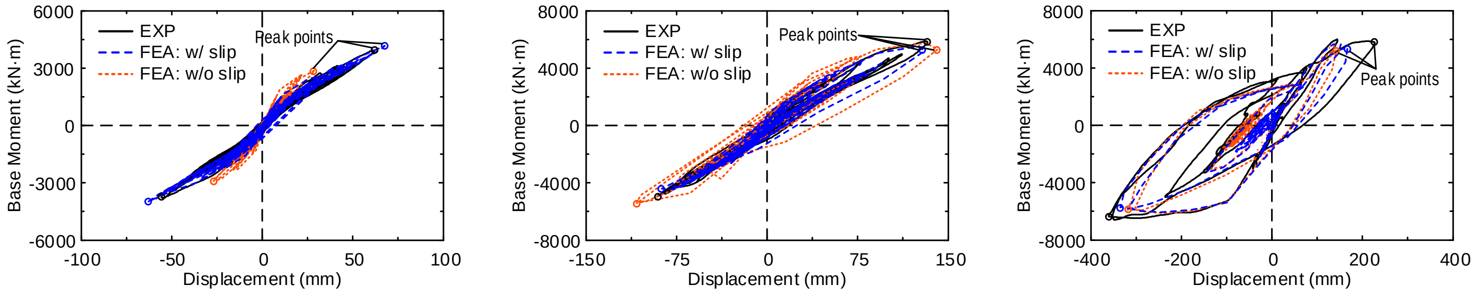

(a) EQ1 (b) EQ2 (c) EQ3

Fig. 9 – Comparison of column response in terms of base moment and displacement

Fig. 10 compares the measured column responses in terms of base moment and base curvature with the numerical results. Comparisons of the curves indicate the good accuracy of the developed model in simulating the column responses at a sectional level. The developed model can closely predict the column sectional stiffness, indicating that the rebar fiber strain increment contributed by the anchorage slip are well considered. Therefore, the modified fiber element model is validated at the sectional level. On the contrary, the conventional model without considering the slip effect overestimated the column sectional stiffness, and thus may underestimate or overestimate the column responses during some earthquakes, especially in EQ1 and EQ2 (Figs. 10a and b). Therefore, anchorage slip effect should be considered while simulating RC column base sectional responses under earthquakes.

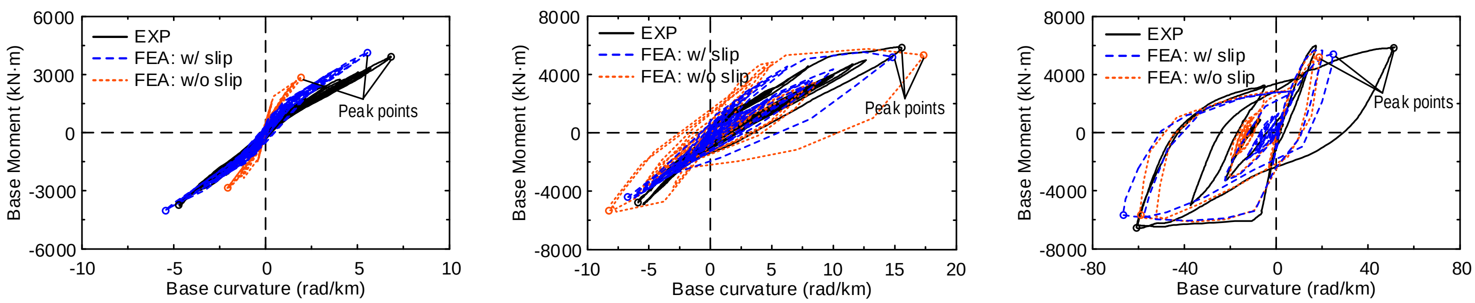

(a) EQ1 (b) EQ2 (c) EQ3

Fig. 10 – Comparison of column response in terms of base moment and curvature

3.3 Fixed-end rotation ratio

From the above comparisons of the experimental and numerical results, the reliability of the developed fiber element model in simulating the column responses at both structural and sectional levels has been validated. To further validate this model at the micro level, the experimental results for the fixed-end rotation ratio at peak displacements are compared with the numerical results.

Fig. 11 compares the measured fixed-end rotation ratio with the numerical results in each test, which are obtained by the developed fiber model considering anchorage slip effect. The red lines represent the experimental results of the fixed-end rotation ratio at peak displacements. The numerical results for the fixed-end rotation ratio converge to a stable value in each loading direction of all earthquake simulations. At relatively high displacements, the fixed-end rotation ratios predicted by the developed model match closely with the test results. The well-prediction of the fixed-end rotation ratio indicates that the rebar anchorage slip is accurately considered in the developed model. Therefore, the model is further validated at the micro level.

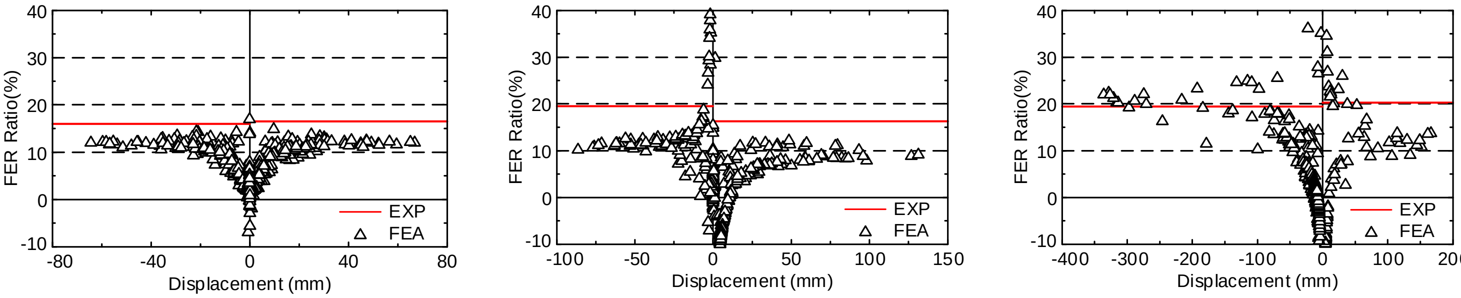

(a) EQ1 (b) EQ2 (c) EQ3

Fig. 11 – Comparison of fixed-end rotation ratio

4. Conclusions

This paper presents a fiber beam–column element model that considers anchorage slip in the footing. The model is then applied to simulate the responses of a full-scale bridge column under shake-table excitations. The main findings in the present study are summarized as follows:

(1) The fiber model considering anchorage slip effect is developed by assuming the stress–total strain (σ–ε_{total}) relationship for the modified uniaxial constitutive law of rebar in the footing fiber element. In the calculation, the total strain is computed as the sum of the rebar deformation and the anchorage slip, which is formulated on the basis of Sezen and Setlzer's macro model [7] and is assumed to be uniformly distributed in the rebar fiber of the footing element.

(2) For the column displacement time-history results, the developed fiber model shows good accuracy in simulating the early stage of each earthquake simulation test, whereas the conventional fiber model may vary significantly from the test results in low-intensity earthquakes.

(3) The developed fiber model can closely predict the column responses at both structural (base moment–column displacement responses) and sectional (base moment–curvature responses) levels.

(4) The developed model is able to predict the fixed-end rotation ratio in each test with a reasonable level of accuracy. Therefore, the well-consideration of the bond-slip effect is further validated.

5. Acknowledgements

The writers gratefully acknowledge the financial support provided by the Tsinghua University Initiative Scientific Research Program (grant number 20161080107) and the National Science Fund of China (grant number 51378291).

6. Copyrights

7. References

[1] Schoettler MJ, Restrepo JI, Guerrini G, Duck DE, Carrea F (2015): A full-scale, single-column bridge bent tested by shake-table excitation. *PEER Report 2015/02*, Pacific Earthquake Engineering Research Center (PEER), Berkeley, USA.

[2] Terzic V, Schoettler MJ, Restrepo JI, Mahin SA (2015): Concrete column blind prediction contest 2010: Outcomes and observations. *PEER Report 2015/01*, Pacific Earthquake Engineering Research Center (PEER), Berkeley, USA.

[3] Pacific Earthquake Engineering Research Center (2010): *Concrete Column Blind Prediction Contest 2010*. http://nisee2.berkeley.edu/peer/prediction_contest.

[4] Blandón C (2012): Sensibility of nonlinear time history analysis of a RC column using large scale shaking table results as benchmark. *15th World Conference on Earthquake Engineering*, Lisbon, Portugal.

[5] Sezen H, Moehle JP (2006): Seismic tests of concrete columns with light transverse reinforcement. *ACI Structural Journal*, **103** (6): 842–849.

[6] Alsiwat JM, Saatcioglu M (1992): Reinforcement anchorage slip under monotonic loading. *Journal of Structural Engineering*, **118** (9): 2421–2438.

[7] Sezen H, Setzler EJ (2008): Reinforcement slip in reinforced concrete columns. *ACI Structural Journal*, **105** (3): 280–289.

[8] Filippou FC, Popov EP, Bertero VV (1983): Effects of bond deterioration on hysteretic behavior of reinforced concrete joints. *Report UCB/EERC 83/19*, Earthquake Engineering Research Center, Berkeley, USA.

[9] Monti G, Filippou FC, Spacone E (1997): Finite element for anchored bars under cyclic load reversals. *Journal of Structural Engineering*, **123** (5): 614–623.

[10] Monti G, Spacone E (2000): Reinforced concrete fiber beam element with bond–slip. *Journal of Structural Engineering*, **126** (6): 654–661.

[11] Eligehausen R, Popov EP, Bertero VV (1983): Local bond stress–slip relationships of deformed bars under generalized excitations. *Report UCB/EERC 83/23*, Earthquake Engineering Research Center, Berkeley, USA.

[12] Saatcioglu M, Alsiwat JM, Ozcebe G (1992): Hysteretic behavior of anchorage slip in R/C members. *Journal of Structural Engineering*, **118** (9): 2439–2458.

[13] Sezen H, Chowdhury T (2009): Hysteretic model for reinforced concrete columns including the effect of shear and axial load failure. *Journal of Structural Engineering*, **135** (2): 139–146.

[14] Zhao J, Sritharan S (2007): Modeling of strain penetration effects in fiber-based analysis of reinforced concrete structures. *ACI Structural Journal*, **104** (2): 133–141.

[15] Spacone E, Filippou FC, Taucer FF (1996): Fibre beam–column model for non-linear analysis of R/C frames: Part I. Formulation. *Earthquake Engineering & Structural Dynamics*, **25** (7): 711–725.

[16] Taucer F, Spacone E, Filippou FC (1991): A fiber beam–column element for seismic response analysis of reinforced concrete structures. *Report UCB/EERC 91/17*, Earthquake Engineering Research Center, Berkeley, USA.

[17] Tao MX, Nie JG (2014): Fiber beam–column model considering slab spatial composite effect for nonlinear analysis of composite frame systems. *Journal of Structural Engineering*, **140** (1): 04013039.

[18] Tao MX, Nie JG (2015): Element mesh, section discretization and material hysteretic laws for fiber beam–column elements of composite structural members. *Materials and Structures*, **48** (8): 2521–2544.

[19] MSC.Software Corporation (2012): *MSC.Marc 2012 Volume A: Theory and User Information*. Santa Ana, USA.

[20] Esmaeily A, Xiao Y (2005): Behavior of reinforced concrete columns under variable axial loads: analysis. *ACI Structural Journal*, **102** (5): 736–744.

[21] Légeron F, Paultre P, Mazars J (2005): Damage mechanics modeling of nonlinear seismic behavior of concrete structures. *Journal of Structural Engineering*, **131** (6): 946–955.

[22] Coleman J, Spacone E (2001): Localization issues in force-based frame elements. *Journal of Structural Engineering*, **127** (11): 1257–1265.

[23] Zahn FA (1985): *Design of reinforced concrete bridge columns for strength and ductility*. Ph. D. thesis, University of Canterbury, Christchurch, New Zealand.